Power Generation Hot Paper

International Edition: DOI: 10.1002/anie.201706620
German Edition: DOI: 10.1002/ange.201706620

A One-Dimensional Fluidic Nanogenerator with a High Power Conversion Efficiency

*Yifan Xu+, Peining Chen+, Jing Zhang, Songlin Xie, Fang Wan, Jue Deng, Xunliang Cheng, Yajie Hu, Meng Liao, Bingjie Wang, Xuemei Sun, and Huisheng Peng**

Abstract: *Electricity generation from flowing water has been developed for over a century and plays a critical role in our lives. Generally, heavy and complex facilities are required for electricity generation, while using these technologies for applications that require a small size and high flexibility is difficult. Here, we developed a fluidic nanogenerator fiber from an aligned carbon nanotube sheet to generate electricity from any flowing water source in the environment as well as in the human body. The power conversion efficiency reached 23.3 %. The fluidic nanogenerator fiber was flexible and stretchable, and the high performance was well-maintained after deformation over 1 000 000 cycles. The fiber also offered unique and promising advantages, such as the ability to be woven into fabrics for large-scale applications.*

Owing to the increasingly severe energy crisis, harvesting energy from the environment has become a dominant energy source.[1–4] Flowing water is one of the most accessible forms of energy in nature, as water is available in streams, rivers, lakes and oceans in the environment as well as in tissue fluids and blood in our bodies.[5–8] Power generation from flowing processes can proceed stably and continuously, unlike other energy sources such as wind energy, which is dramatically affected by the weather, and solar energy, which is available only during the day.[9–12] Thus, over the past century, people have built water wheels and large dams to harvest the enormous mechanical energy from flowing processes. However, heavy and complex facilities are required to harness flowing processes, which may be unavailable for various working conditions requiring a small size and high flexibility.

Herein, a fiber-shaped fluidic nanogenerator (FFNG) that is lightweight, flexible and stretchable was fabricated from an aligned multi-walled carbon nanotube (MWCNT) sheet. The MWCNT sheet was designed as both the active and electrode material because of its excellent electronic and mechanical properties. The FFNG efficiently worked within various forms of flowing water in the environment and in the human body, and the generated electricity was controllable by varying the ion species, concentration, temperature and flowing velocity of the fluid. The fiber shape also offered unique and promising advantages. For instance, the FFNG could be woven into textiles to enhance the harvested energy for large-scale applications.

The aligned MWCNT sheet was drawn from a spinnable MWCNT array and continuously wrapped onto a polymer fiber (Figure 1 a,b). The FFNG was also prepared by twisting the MWCNT sheet into a MWCNT fiber. The aligned MWCNT sheets and fibers showed high electrical conductivities of 10^2–10^3 S cm^{-1} and tensile strengths of 10^2–10^3 MPa.[13–15] Here, the MWCNT/polymer fiber was taken as a proof of concept. The MWCNTs were compactly covered on the polymer substrate with a highly aligned structure (Figure 1 c). With a typical thickness of 18 nm for a single layer of the MWCNT sheet, a total thickness of approximately 260 nm was typically obtained by repeating the wrapping process.[16] The diameter of the resulting fiber was readily controlled by the polymer substrate. For the convenience of this discussion, a diameter of 800 μm was studied unless otherwise specified. The resistance of the FFNG was 0.94 kΩ cm^{-1} in dry state according to the I–V curve (see Figures S1 and S2 in the Supporting Information).

A NaCl solution, as one of the most common electrolytes both in sea water and biological fluids, was first adopted as a candidate to systematically study the electric signal generation of the FFNG. The FFNG was fixed at the center of a tube with two copper wires attached to the ends (Figure 1 d). When a NaCl solution was injected into the tube from one end and flowed through the FFNG surface at a velocity of 1.2 cm s^{-1}, an output voltage was rapidly generated as the solution contacted the FFNG. Along with an increasing flow distance (i.e., immersed length of the FFNG in NaCl), the output voltage gradually increased towards a peak value and then returned to the original voltage upon backflow at the same velocity (Figure 2 a). If the NaCl solution was injected into the tube from the other end, the direction of the output voltage would be reversed. However, the output voltage of the FFNG was rather low in the flowing solution when the whole device was immersed, since the contact length between the FFNG and the solution no longer increased (Figure S3). With an increasing flow velocity from 2.6 to 195 cm s^{-1} of a 0.6 M NaCl solution, the output voltage increased from 42 to 121 mV (Figure 2 b). At a velocity of 12.9 cm s^{-1}, the voltage was further enhanced by increasing

[*] Y. Xu,[+] Dr. P. Chen,[+] J. Zhang, S. Xie, J. Deng, Dr. X. Cheng, Y. Hu, M. Liao, Dr. B. Wang, Dr. X. Sun, Prof. Dr. H. Peng
State Key Laboratory of Molecular Engineering of Polymers
Department of Macromolecular Science and
Laboratory of Advanced Materials, Fudan University
Shanghai 200438 (China)
E-mail: penghs@fudan.edu.cn
Dr. F. Wan
Sports Medicine Centre, Huashan Hospital
Department of Sports Medicine and Arthroscopy Surgery, Fudan University
Shanghai 200040 (China)
[+] These authors contributed equally to this work.

Supporting information for this article can be found under: https://doi.org/10.1002/anie.201706620.

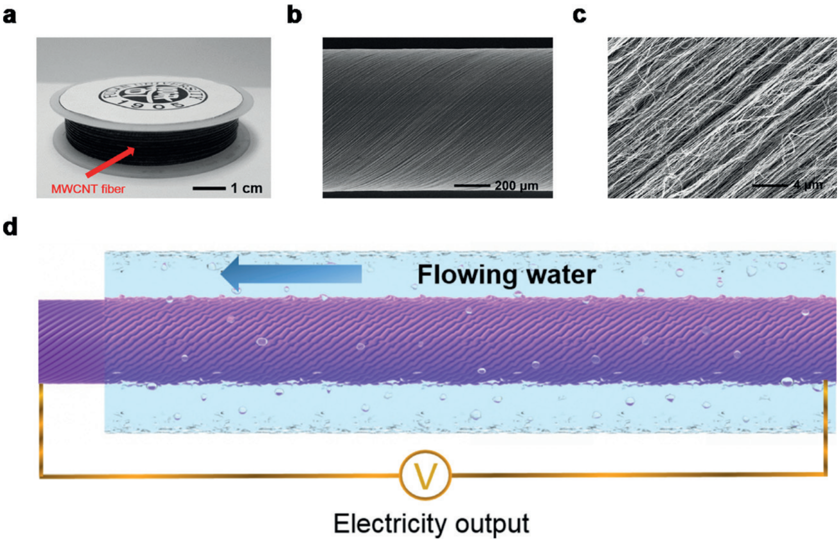

Figure 1. Structure characterization and measurement illustration of the FFNG. a) Photograph of a continuous FFNG based on MWCNTs with a diameter of 0.8 mm in a roll. b,c) Side-view scanning electron microscopy (SEM) images of the FFNG at low and high magnifications, respectively. d) Schematic illustration of the experimental setup of measuring the electricity output in flowing water.

the NaCl concentration, achieving a maximal value of 151.5 mV at a concentration of 4 M (Figure 2c). The FFNG output current response to flowing water was also studied, and similar trends of the voltage versus concentration were observed.

We further discovered that the flow-induced electric output could be greatly enhanced by introducing ordered mesoporous carbon (OMC) (Figure S4). As described in the Experimental Section, OMC particles were incorporated into the interlayer among the MWCNT sheets to obtain an OMC-incorporated FFNG (Figure S5). A highly uniform and ordered mesoporous structure (pore sizes of 3–5 nm) was shown, resulting in a high specific surface area ($>900\ m^2 g^{-1}$) (Figure S6). The output voltage and current of the OMC-incorporated FFNG could be sustained for over 1 h, showing a stable electricity generation (Figures S7 and S8). The output voltage was efficiently improved, reaching a maximal value of 341 mV with an increased OMC content from 0 to 5.1 $\mu g\, cm^{-1}$ (Figure 2d). This achieved maximal value was two times higher than that of the OMC-free FFNG. The output voltage remained almost unchanged when the OMC content exceeded 10.2 $\mu g\, cm^{-1}$. Similar to the OMC-free FFNG, the electric output generated by the OMC-incorporated FFNG was also efficiently improved by either increasing the NaCl concentration or the flow velocity (Figure S9). A maximal electric output with a voltage of 0.3 V and a current of 0.06 mA was achieved. The output current is two or three orders of magnitude higher than that of typical piezoelectric and triboelectric nanogenerators with similar dimensions.[17,18] Additionally, an enhanced output voltage was generated at a higher operating temperature. For instance, as the operating temperature was increased from 10 to 90 °C, approximately linear increases of the output voltages from 2.8 to 22.5 mV and 78 to 119.5 mV were observed for the FFNGs without and with OMC, respectively (Figure S10).

As expected, the electric output was enhanced by increasing the FFNG length. The output voltage linearly rose from 7.7 to 85.8 mV upon lengthening the FFNG from 2 to 20 cm (Figure S11). A similar trend was observed for the OMC-incorporated FFNG. An output voltage of 650 mV and a current of 67 μA were produced by a 30-cm-long OMC-incorporated FFNG (Figure S12). Furthermore, the output electricity was further improved and well controlled by connecting the FFNGs in series and parallel (Figure S13). Output voltage of 200 V and current of 25 mA may be produced from a thousand FFNG units in series and in parallel, respectively (Figure S14). The dependences of the output voltage and current on the load were studied by connecting the OMC-incorporated FFNG to an external resistor. A maximal power density of 39.5 $mW\, g^{-1}$ occurred at 3 kΩ (Figure S15). The power curve of the FFNG in a saturated NaCl solution flowing from one end to the other was obtained by the output voltage and current at an external resistor of 3 kΩ, and the power conversion efficiency was calculated as 23.3 % accordingly (Experimental Section and Figure S16).

In general, the electricity was derived from the relative movement between the FFNG and the solution. Herein, the occurrence of electricity generation was predictable by moving the FFNG in a quiet fluid. For instance, a peak output voltage of 120 mV was generated by dipping the OMC-incorporated FFNG into a saturated NaCl solution. The output voltage generation was highly flexible and stable and showed no obvious decrease over 1 000 000 bending cycles (Figure 2e). Stable performance of the FFNG was also achieved after other more complex deformations, such as twisting. Moreover, the contact angle between the FFNG and the fluid had little effect on the output voltage, displaying the capability of harvesting electric energy from fluids at various directions in nature (Figure S17).

Recently, stretchable energy harvesting devices have attracted increasing attention because of their promising applications in portable and wearable electronics. A stretchable FFNG was fabricated from an elastic fiber substrate (see the Experimental Section). The electrical resistance of the FFNG remained almost unchanged under stretching (Figure S18). An electric output was produced by stretching the elastic FFNG half-immersed in saline water (Figure S19a), and a stable peak output voltage of 33 mV was generated under a stretching frequency of 0.67 Hz (Figure S19b). For the elastic OMC-incorporated FFNG, similar electricity generation behavior was observed, and the peak output voltage was enhanced after the incorporation of OMC (Figure S20). The electricity generation resulted from the relative movement between the MWCNT and the fluid during

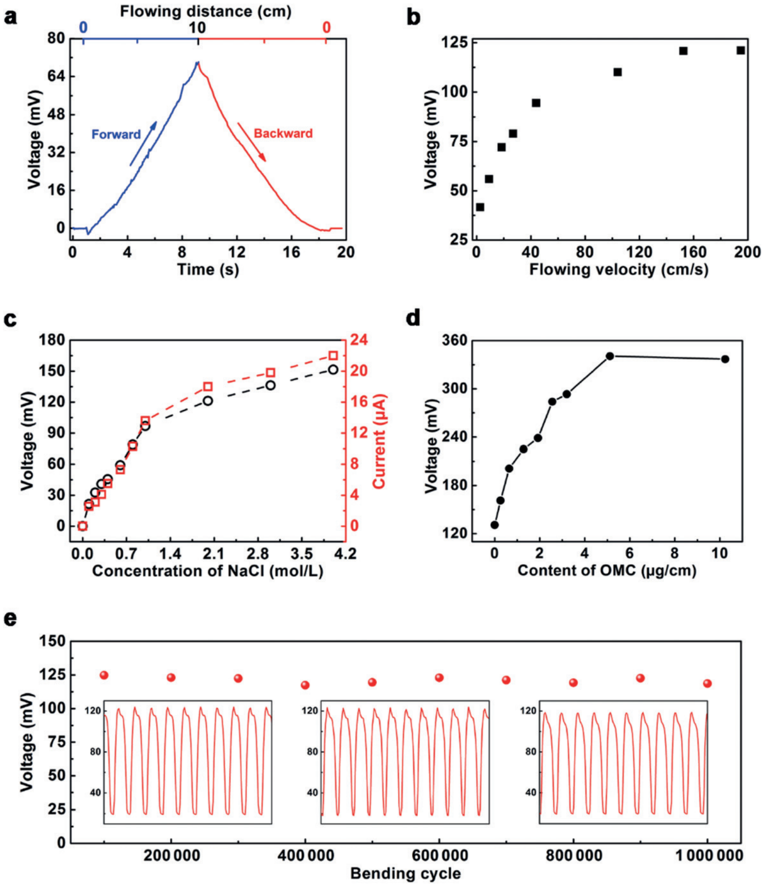

Figure 2. Electricity produced by the FFNG with flowing saline water at the surface. a) Output voltage of a reciprocating flow of a saturated NaCl solution at 1.2 $cm\,s^{-1}$. b) Dependence of the output voltage on the velocity of a flowing 0.6 M NaCl solution. c) Dependences of the output voltage and current on the concentration of a NaCl solution (flowing velocity was 12.9 $cm\,s^{-1}$). d) Dependence of the output voltage on the OMC content of an OMC-incorporated FFNG in a saturated NaCl solution (the flowing velocity was 20 $cm\,s^{-1}$). e) Output voltage generated by repeatedly dipping an OMC-incorporated FFNG into a NaCl solution with an increasing number of bending cycles. The inserted graphs show the output voltages of the FFNG after 200000, 600000 and 1000000 bending cycles in the NaCl solution. The FFNG length in (a–e) is 10 cm.

the stretching process, where the amount of MWCNT immersed in the solution decreased and increased during the stretching and relaxing process, respectively. The peak output voltage was enhanced by increasing the stretching frequency from 0.17 to 1.33 Hz, that is, the relative speed between the MWCNT and the fluid was increased from 2.7 to 21.3 $cm\,s^{-1}$ (Figure S21 and S22). The voltage baseline rose along with the increase in the stretching frequency, possibly because the baseline needed more time to release charge at higher stretching frequencies, which will be discussed below. Interestingly, the peak output voltage of the FFNG was also efficiently and linearly improved from 17.8 to 58.6 mV by increasing the immersion depth from 2.5 to 7.5 cm (Figure S23). This phenomenon may be used to monitor water level variations without an external power supply.

Regarding harvesting energy from biological fluids, adapting generators for miniature stream-like channels existing in the human body is essential and challenging, as these miniature channels apparently differ from free bulk solutions for most current fluidic generators. The FFNG in this work can be desirably implemented to harvest flowing energy of biological fluids, such as blood, in a one-dimensional channel. For demonstration, the FFNG was stabilized in a vessel-like tube to mimic flowing blood at various velocities (Figure S24). Output voltages of 40.6, 28.4 and 4.3 mV were observed for the artery (17 $cm\,s^{-1}$), vein (7 $cm\,s^{-1}$) and capillary (0.04 $cm\,s^{-1}$), respectively. The FFNG also effectively worked in phosphate-buffered saline (PBS). When flowing 0.01 and 0.1 M PBS at 20 $cm\,s^{-1}$, FFNG output voltages of 61 and 173 mV, respectively, were obtained (Figure S25).

Other types of miniature energy harvesting devices, such as one-dimensional solar cells[16,19–22] and electrostatic and triboelectric nanogenerators,[23–26] have been previously investigated. For solar cells, only one side can be illuminated to harvest sunlight during use. Additionally, the availability of sunlight is only during daytime. For electrostatic and triboelectric nanogenerators, the output currents are relatively low,[27,28] and the power conversion efficiencies largely decay in moist environments. Furthermore, it is hard to apply external friction force on the curved surface of a single fiber, and the surface cannot be fully utilized to harvest triboelectric energy, leading to a relatively low harvesting performance. Importantly, flowing energy can be used during both day and night time and is not affected by weather. To systematically estimate the harvesting performance of the FFNG, a comparison with various miniature fiber-shaped generators, including dye-sensitized solar cells (DSSCs),[19,29–33] perovskite solar cells (PSCs),[20,21,34–36] quantum-dot-sensitized solar cells (QDSSCs),[37–39] organic solar cells (OSCs),[40,41] inorganic solar cells (ISCs)[42,43] and nanogenerators (NGs) that harvest electrostatic and triboelectric energy,[23,24] was further conducted (Figure 3). The FFNG showed the highest power conversion efficiency of 23.3%. Furthermore, the FFNG is highly flexible and stable, and can bear millions of deformation cycles in water.

Unlike previous work where two electrodes were completely immersed in the solution,[44,45] only one electrode of the FFNG contacted the solution, and the output voltage went down immediately when the two electrodes were both immersed. It cannot be explained by previously proposed mechanism, since the curved shape of the output voltage was different and showed better repeatability for the FFNG. An electric double layer (EDL) model is summarized for the working mechanism of the FFNG. When the FFNG comes into contact with the solution, an EDL forms between the surface of the immersed MWCNT and the solution (Figure 4a). The zeta potential of the MWCNT in deionized water was measured as −12.5 mV, indicating a negative surface of the MWCNT (Figure S26). A stern layer was formed by the

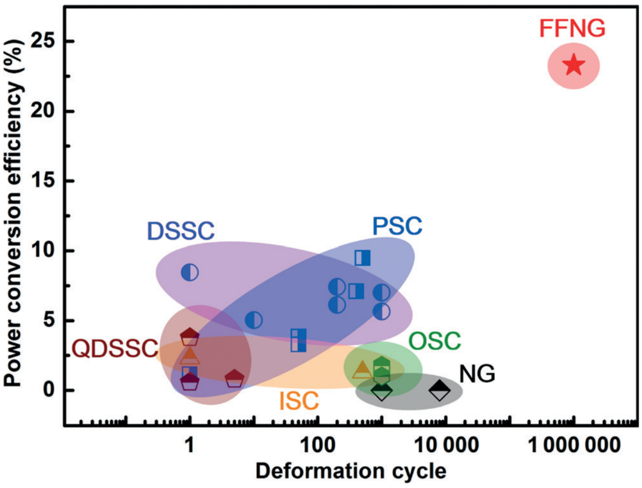

Figure 3. Power conversion efficiencies and flexibilities of the FFNG and other fiber-shaped generators, including dye-sensitized solar cells (DSSCs),[19,25–29] perovskite solar cells (PSCs),[20,21,30–32] quantum-dot-sensitized solar cells (QDSSCs),[33–35] organic solar cells (OSCs),[36,37] inorganic solar cells (ISCs)[38,39] and nanogenerators (NGs) that harvest electrostatic and triboelectric energy.[23,24].

cations adsorbed onto the MWCNT because of the negative zeta potential. However, the anions in the diffusion layer were retarded in migration to counteract the net charge of the stern layer;[46,47] therefore, the electrons were drawn from the MWCNT to balance the excess charge, thus inducing a potential difference. As the contact length between the FFNG and the solution rapidly increased, further unbalanced charge accumulated at the front half (Figure S27), and a higher potential difference was thus generated. When the contact length of the FFNG with the solution ceased to rise, the ions in the solution gradually balanced the excess charge and the voltage decreased. It is worth noting that the output voltage and current did not return to zero after the solution stopped flowing. Sealing the electrodes decreased the output voltage of the FFNG. It could probably be attributed to the galvanic nature of metal–carbon nanomaterial junction which also contributed to the electricity generation.[48] Furthermore, as the interspace of the MWCNT was small, the voltage output contribution of the capillary force-driving water flow among the MWCNTs had been also taken into consideration.[49,50] However, owing to the hydrophobic property of the MWCNT, water cannot go into the interspace of the MWCNTs efficiently.[14] The streaming potential by pressure-driving water flow is hard to be induced on hydrophobic surface.[49] Therefore, the effect of the capillary force-driving water flow might be neglected in the flowing electricity generation.

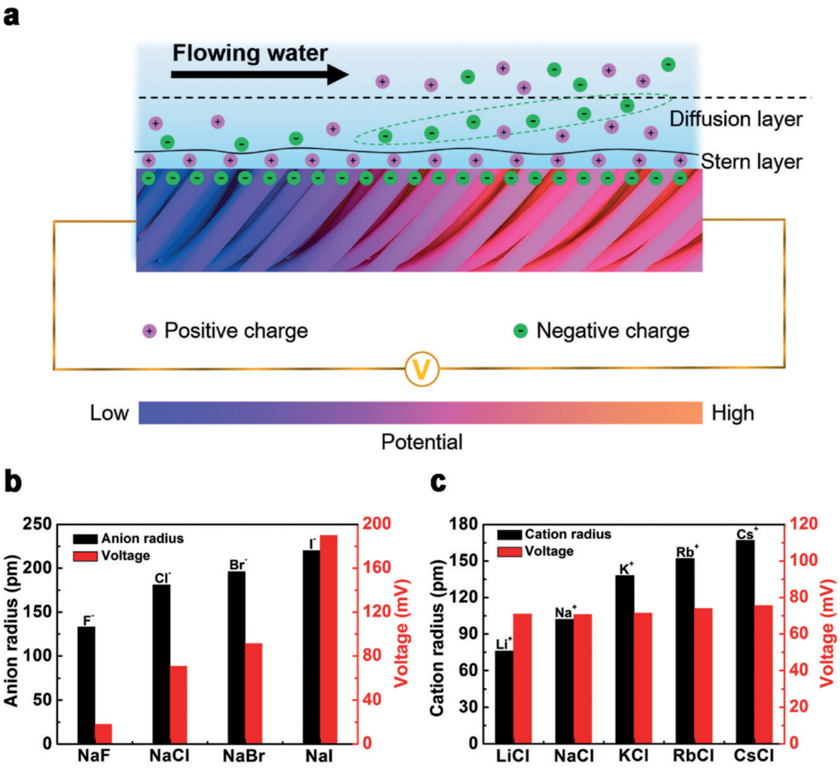

Figure 4. Mechanism of the FFNG. a) Schematic illustration of the mechanism showing the flow potential in the FFNG. An EDL is formed on the surface of the MWCNT in the fluid. The anions at the front end of the flowing water could not immediately counteract the net charge of the stern layer. Then, the charge imbalance between the anions and cations draws electrons from the MWCNT to balance the excess charges, generating a potential difference along the FFNG. b) Output voltages by dipping the OMC-incorporated FFNG into NaF, NaCl, NaBr and NaI solutions with the same concentration of 0.6 M. c) Output voltages by dipping the OMC-incorporated FFNG into LiCl, NaCl, KCl, RbCl and CsCl solutions with the same concentration of 0.6 M. The OMC content was 5.1 $\mu g\,cm^{-1}$ in (b) and (c).

For the OMC-incorporated FFNG, owing to the large surface area, the OMC provides a higher capacity for ion adsorption, which allows for the generation of a larger potential difference. To verify this hypothesis, we investigated the cyclic voltammograms of the FFNG with increasing OMC contents in a three-electrode electrochemical cell. No cathodic or anodic peaks were observed, indicating typical EDL behavior. The area of the CV curve, which represents the capacitance, increased with an increasing OMC content from 0 to 5.1 $\mu g\,cm^{-1}$, which is consistent with the increasing output voltage of the FFNG (Figure S28). The capacity for charge adsorption was susceptible to the environmental temperature. The areas of the CV curves, that is, capacitances, increased at higher operating temperatures (Figures S29 and S30), thus generating higher voltages. Additionally, the adsorption behavior was also affected by the ion size. Anions with larger radii were not easily attracted to the stern layer because of their weaker electronegativity and larger volumes, thus increasing the output voltage (Figures 4b and S31a). The variation of cations with different radii showed little influence on the output voltage (Figures 4c and S31b).

To demonstrate a practical application, the FFNG was placed in sea water to harvest the flowing energy from natural movements, such as sea waves (Figure S32). To harvest the mechanical energy from wind above stagnant water, the FFNG was also tied to the axis of a fan (Figure S33 a). When the fan was driven by the wind, the FFNG moved up and down repeatedly. An output voltage of approximately 60 mV was continuously produced through the relative movement between the FFNG and the sea (Figure S33 b). To demonstrate an application in the body, one terminal electrode of the FFNG was attached to a sciatic nerve of a frog. The other end was connected to the nerve with a switch, and a force sensor was connected to the gastrocnemius muscle to detect the contraction through a thread (Figure S34). Under the flow-induced electric stimulation, a tension force of 5.7 mN was generated through muscle contraction (Figure S35), and a continuous generation of tension was obtained with good reproducibility.

To summarize, we create a new family of FFNGs to harvest flowing energy from any flowing water in the environment. With the one-dimensional structure, it can desirably be implemented in the human body and turn the flowing of body fluids and blood into electricity. A maximal power conversion efficiency of 23.3 % can de achieved by the FFNG, which much surpasses all previously reported fiber-shaped energy harvesting devices. It also demonstrates both high stability and durability. For example, the harvesting performance has been well-maintained even after 1 000 000 cycles of deformation. This new method may provide a general and effective paradigm in the development of highly efficient and miniaturized power systems.

Acknowledgements

This work was supported by MOST (2016YFA0203302), NSFC (21634003, 51573027, 51403038, 51673043, and 21604012) and STCSM (16JC1400702, 15XD1500400, and 15JC1490200).

Conflict of interest

The authors declare no conflict of interest.

Keywords: carbon nanotubes · fiber-shaped devices · fluidic nanogenerators · nanomaterials · power generation

How to cite: *Angew. Chem. Int. Ed.* **2017**, *56*, 12940–12945
Angew. Chem. **2017**, *129*, 13120–13125

[1] Y. Chen, D. Liang, X. P. A. Gao, J. I. D. Alexander, *Nano Lett.* **2013**, *13*, 3953–3957.
[2] J. Feng, M. Graf, K. Liu, D. Ovchinnikov, D. Dumcenco, M. Heiranian, V. Nandigana, N. R. Aluru, A. Kis, A. Radenovic, *Nature* **2016**, *536*, 197–200.
[3] R. Zhang, S. Wang, M.-H. Yeh, C. Pan, L. Lin, R. Yu, Y. Zhang, L. Zheng, Z. Jiao, Z. L. Wang, *Adv. Mater.* **2015**, *27*, 6482–6487.
[4] W. Guo, C. Cheng, Y. Wu, Y. Jiang, J. Gao, D. Li, L. Jiang, *Adv. Mater.* **2013**, *25*, 6064–6068.
[5] S. Ghosh, A. K. Sood, N. Kumar, *Science* **2003**, *299*, 1042–1044.
[6] B. Bourlon, J. Wong, C. Miko, L. Forro, M. Bockrath, *Nat. Nanotechnol.* **2007**, *2*, 104–107.
[7] Q. Yuan, Y.-P. Zhao, *J. Am. Chem. Soc.* **2009**, *131*, 6374–6376.
[8] Y. Zhao, L. Song, K. Deng, Z. Liu, Z. Zhang, Y. Yang, C. Wang, H. Yang, A. Jin, Q. Luo, C. Gu, S. Xie, L. Sun, *Adv. Mater.* **2008**, *20*, 1772–1776.
[9] Y. Su, X. Wen, G. Zhu, J. Yang, J. Chen, P. Bai, Z. Wu, Y. Jiang, Z. L. Wang, *Nano Energy* **2014**, *9*, 186–195.
[10] Z. L. Wang, *ACS Nano* **2013**, *7*, 9533–9557.
[11] H. G. Park, Y. Jung, *Chem. Soc. Rev.* **2014**, *43*, 565–576.
[12] W. Huang, G. Wang, F. Gao, Z. Qiao, G. Wang, M. Chen, Y. Deng, L. Tao, Y. Zhao, X. Fan, L. Sun, *J. Phys. Chem. C* **2014**, *118*, 8783–8787.
[13] M. F. L. De Volder, S. H. Tawfick, R. H. Baughman, A. J. Hart, *Science* **2013**, *339*, 535–539.
[14] P. N. Chen, Y. F. Xu, S. S. He, X. M. Sun, S. W. Pan, J. Deng, D. Y. Chen, H. S. Peng, *Nat. Nanotechnol.* **2015**, *10*, 1077–1083.
[15] Y. Xu, Y. Zhang, Z. Guo, J. Ren, Y. Wang, H. Peng, *Angew. Chem. Int. Ed.* **2015**, *54*, 15390–15394; *Angew. Chem.* **2015**, *127*, 15610–15614.
[16] Z. B. Yang, J. Deng, X. M. Sun, H. P. Li, H. S. Peng, *Adv. Mater.* **2014**, *26*, 2643–2647.
[17] X. Li, Z.-H. Lin, G. Cheng, X. Wen, Y. Liu, S. Niu, Z. L. Wang, *ACS Nano* **2014**, *8*, 10674–10681.
[18] H. Guo, M.-H. Yeh, Y.-C. Lai, Y. Zi, C. Wu, Z. Wen, C. Hu, Z. L. Wang, *ACS Nano* **2016**, *10*, 10580–10588.
[19] Z. Yang, H. Sun, T. Chen, L. Qiu, Y. Luo, H. Peng, *Angew. Chem. Int. Ed.* **2013**, *52*, 7545–7548; *Angew. Chem.* **2013**, *125*, 7693–7696.
[20] L. Qiu, J. Deng, X. Lu, Z. Yang, H. Peng, *Angew. Chem. Int. Ed.* **2014**, *53*, 10425–10428; *Angew. Chem.* **2014**, *126*, 10593–10596.
[21] L. Qiu, S. He, J. Yang, J. Deng, H. Peng, *Small* **2016**, *12*, 2419–2424.
[22] X. Fan, Z. Chu, F. Wang, C. Zhang, L. Chen, Y. Tang, D. Zou, *Adv. Mater.* **2008**, *20*, 592–595.
[23] X. Yu, J. Pan, J. Zhang, H. Sun, S. He, L. Qiu, H. Lou, X. Sun, H. Peng, *J. Mater. Chem. A* **2017**, *5*, 6032–6037.
[24] X. Yu, J. Pan, J. Deng, J. Zhou, X. Sun, H. Peng, *Adv. Mater.* **2016**, *28*, 10744–10749.
[25] J. Wang, X. Li, Y. Zi, S. Wang, Z. Li, L. Zheng, F. Yi, S. Li, Z. L. Wang, *Adv. Mater.* **2015**, *27*, 4830–4836.
[26] X. Pu, W. Song, M. Liu, C. Sun, C. Du, C. Jiang, X. Huang, D. Zou, W. Hu, Z. L. Wang, *Adv. Energy Mater.* **2016**, *6*, 1601048.
[27] J. Zhong, Y. Zhang, Q. Zhong, Q. Hu, B. Hu, Z. L. Wang, J. Zhou, *ACS Nano* **2014**, *8*, 6273–6280.
[28] X. He, Y. Zi, H. Guo, H. Zheng, Y. Xi, C. Wu, J. Wang, W. Zhang, C. Lu, Z. L. Wang, *Adv. Funct. Mater.* **2017**, *27*, 1604378.
[29] A. Ali, S. M. Shah, S. Bozar, M. Kazici, B. Keskin, M. Kaleli, S. Akyurekli, S. Gunes, *Nanotechnology* **2016**, *27*, 384003.
[30] Z. Wen, M.-H. Yeh, H. Guo, J. Wang, Y. Zi, W. Xu, J. Deng, L. Zhu, X. Wang, C. Hu, L. Zhu, X. Sun, Z. L. Wang, *Sci. Adv.* **2016**, *2*, e1600097.
[31] W. Song, H. Wang, G. Liu, M. Peng, D. Zou, *Nano Energy* **2016**, *19*, 1–7.
[32] Z. Lv, J. Yu, H. Wu, J. Shang, D. Wang, S. Hou, Y. Fu, K. Wu, D. Zou, *Nanoscale* **2012**, *4*, 1248–1253.
[33] M. Peng, K. Yan, H. Hu, D. Shen, W. Song, D. Zou, *J. Mater. Chem. C* **2015**, *3*, 2157–2165.
[34] L. Qiu, S. He, J. Yang, F. Jin, J. Deng, H. Sun, X. Cheng, G. Guan, X. Sun, H. Zhao, H. Peng, *J. Mater. Chem. A* **2016**, *4*, 10105–10109.
[35] M. Lee, Y. Ko, Y. Jun, *J. Mater. Chem. A* **2015**, *3*, 19310–19313.
[36] X. Wang, S. A. Kulkarni, Z. Li, W. Xu, S. K. Batabyal, S. Zhang, A. Cao, L. H. Wong, *Nanotechnology* **2016**, *27*, 20LT01.
[37] H. Chen, L. Zhu, M. Wang, H. Liu, W. Li, *Nanotechnology* **2011**, *22*, 475402.

[38] H. Liu, G. Zhang, J. Liang, J. Li, J. Yang, J. Wei, W. Sun, Z. Shen, *IEEE J. Photovolt.* **2016**, *6*, 952–959.

[39] W. Guo, C. Chen, M. Ye, M. Lv, C. Lin, *Nanoscale* **2014**, *6*, 3656–3663.

[40] Z. Zhang, Z. Yang, Z. Wu, G. Guan, S. Pan, Y. Zhang, H. Li, J. Deng, B. Sun, H. Peng, *Adv. Energy Mater.* **2014**, *4*, 1301750.

[41] Z. Zhang, X. Chen, P. Chen, G. Guan, L. Qiu, H. Lin, Z. Yang, W. Bai, Y. Luo, H. Peng, *Adv. Mater.* **2014**, *26*, 466–470.

[42] L. Zhang, L. Song, Q. Tian, X. Kuang, J. Hu, J. Liu, J. Yang, Z. Chen, *Nano Energy* **2012**, *1*, 769–776.

[43] N. Zhang, J. Chen, Y. Huang, W. Guo, J. Yang, J. Du, X. Fan, C. Tao, *Adv. Mater.* **2016**, *28*, 263–269.

[44] P. Dhiman, F. Yavari, X. Mi, H. Gullapalli, Y. Shi, P. M. Ajayan, N. Koratkar, *Nano Lett.* **2011**, *11*, 3123–3127.

[45] J. Yin, Z. Zhang, X. Li, J. Zhou, W. Guo, *Nano Lett.* **2012**, *12*, 1736–1741.

[46] J. Yin, X. M. Li, J. Yu, Z. H. Zhang, J. X. Zhou, W. L. Guo, *Nat. Nanotechnol.* **2014**, *9*, 378–383.

[47] J. Yin, Z. H. Zhang, X. M. Li, J. Yu, J. X. Zhou, Y. Q. Chen, W. L. Guo, *Nat. Commun.* **2014**, *5*, 3582.

[48] K. Hu, R. Xiong, H. Guo, R. Ma, S. Zhang, Z. L. Wang, V. V. Tsukruk, *Adv. Mater.* **2016**, *28*, 3549–3556.

[49] G. Xue, Y. Xu, T. Ding, J. Li, J. Yin, W. Fei, Y. Cao, J. Yu, L. Yuan, L. Gong, J. Chen, S. Deng, J. Zhou, W. Guo, *Nat. Nanotechnol.* **2017**, *12*, 317–321.

[50] T. Ding, K. Liu, J. Li, G. Xue, Q. Chen, L. Huang, B. Hu, J. Zhou, *Adv. Funct. Mater.* **2017**, *27*, 1700551.

Manuscript received: June 29, 2017
Revised manuscript received: August 10, 2017
Accepted manuscript online: August 26, 2017
Version of record online: September 7, 2017

